11-1-2009

How Much can Guided Modes Enhance Absorption in Thin Solar Cells?

Peter N. Saeta
Harvey Mudd College

Vivian E. Ferry
California Institute of Technology

Domenico Pacifici
California Institute of Technology

Jeremy N. Munday
California Institute of Technology

Harry A. Atwater
California Institute of Technology

How much can guided modes enhance absorption in thin solar cells?

Peter N. Saeta,[1,2] **Vivian E. Ferry,**[2] **Domenico Pacifici,**[2]
Jeremy N. Munday,[2] **and Harry A. Atwater**[2]

[1] *Department of Physics, Harvey Mudd College, Claremont, CA 91711 USA*
[2] *Thomas J. Watson Laboratories of Applied Physics, California Institute of Technology, Pasadena, CA 91125 USA*

saeta@hmc.edu

Abstract: Absorption enhancement in thin metal-backed solar cells caused by dipole scatterers embedded in the absorbing layer is studied using a semi-analytical approach. The method accounts for changes in the radiation rate produced by layers above and below the dipole, and treats incoherently the subsequent scattering of light in guided modes from other dipoles. We find large absorption enhancements for strongly coupled dipoles, exceeding the ergodic limit in some configurations involving lossless dipoles. An antireflection-coated 100-nm layer of a-Si:H on Ag absorbs up to 87% of incident above-gap light. Thin layers of both strong and weak absorbers show similar strongly enhanced absorption.

OCIS codes: (250.5403) Plasmonics; (130.0250) Optoelectronics; (160.3900) Materials: metals; (160.6000) Materials: semiconductor materials; (240.6680) Optics at surfaces: surface plasmons.

References and links

1. W. Shockley and H. J. Queisser, "Detailed balance limit of efficiency of *p-n* junction solar cells," J. Appl. Phys. **32**, 510–519 (1961).
2. C. H. Henry, "Limiting efficiencies of ideal single and multiple energy-gap terrestrial solar-cells," J. Appl. Phys. **51**, 4494–4500 (1980).
3. K. Schick, E. Daub, S. Finkbeiner, and P. Würfel, "Verification of a generalized Planck law for luminescence radiation from silicon solar cells," Appl. Phys. A: Mat. Sci. Proc. **54**, 109–114 (1992).
4. P. Campbell and M. A. Green, "Light trapping properties of pyramidally textured surfaces," J. Appl. Phys. **62**, 243–249 (1987).
5. S. S. Hegedus and X. Deng, "Analysis of optical enhancement in *a*-si *n-i-p* solar cells using a detachable back reflector," Conference Record of the 25th IEEE Photovoltaic Specialists Conference pp. 1061–1064 (1996).
6. H. R. Stuart and D. G. Hall, "Thermodynamic limit to light trapping in thin planar structures," J. Opt. Soc. Am. A **14**, 3001–3008 (1997).
7. H. Stuart and D. G. Hall, "Island size effects in nanoparticle-enhanced photodetectors," Appl. Phys. Lett. **73**, 3815–3817 (1998).
8. B. Soller and D. G. Hall, "Energy transfer at optical frequencies to silicon-based waveguiding structures," J. Opt. Soc. Am. A **18**, 2577–2584 (2001).
9. D. Derkacs, S. H. Lim, P. Matheu, W. Mar, and E. T. Yu, "Improved performance of amorphous silicon solar cells via scattering from surface plasmon polaritons in nearby metallic nanoparticles," Appl. Phys. Lett. **89**, 093103 (2006).
10. K. Nakayama, K. Tanabe, and H. Atwater, "Plasmonic nanoparticle enhanced light absorption in GaAs solar cells," Appl. Phys. Lett. **93**, 121904 (2008).
11. K. R. Catchpole and S. Pillai, "Absorption enhancement due to scattering by dipoles into silicon waveguides," J. Appl. Phys. **100**, 044504 (2006).
12. S. Pillai, K. R. Catchpole, T. Trupke, and M. A. Green, "Surface plasmon enhanced silicon solar cells," J. Appl. Phys. **101**, 093105 (2007).

#116570 - $15.00 USD Received 1 Sep 2009; revised 10 Oct 2009; accepted 11 Oct 2009; published 3 Nov 2009

13. F. J. Beck, A. Polman, and K. R. Catchpole, "Tunable light trapping for solar cells using localized surface plasmons," J. Appl. Phys. **105**, 114310 (2009).
14. V. E. Ferry, L. A. Sweatlock, D. Pacifici, and H. A. Atwater, "Plasmonic nanostructure design for efficient light coupling into solar cells," Nano Lett. **8**, 4391–4397 (2008).
15. C. F. Bohren and D. R. Huffman, *Absorption and Scattering of Light by Small Particles*, A Wiley-Interscience publication (Wiley, 1983).
16. The law of refraction is usually attributed (in English-speaking countries) to the Dutch astronomer and mathematician Willebrord Snel van Royen, which he enunciated in 1621, although some scholars argue that the law was first discovered by Ibn Sahl in 984.
17. M. Born and E. Wolf, *Principles of Optics*, 6th ed. (Cambridge University Press, 1999).
18. E. Yablonovitch and G. D. Cody, "Intensity enhancement in textured optical sheets for solar-cells," IEEE Trans. Electron. Devices **29**, 300–305 (1982).
19. T. Tiedje, E. Yablonovitch, G. D. Cody, and B. G. Brooks, "Limiting efficiency of silicon solar cells," IEEE Trans. Electron. Devices **ED-31**, 711–716 (1984).
20. P. Sheng, "Optical absorption of thin film on a Lambertian reflector substrate," IEEE Trans. Electron. Devices **ED-31**, 634–636 (1984).
21. J. E. Sipe, "The dipole antenna problem in surface physics: a new approach," Surf. Sci. **105**, 498–504 (1981).
22. G. W. Ford and W. H. Weber, "Electromagnetic interactions of molecules with metal surfaces," Phys. Rpt. **113**, 195–287 (1984).
23. H. Benisty, R. Stanley, and M. Mayer, "Method of source terms for dipole emission modification in modes of arbitrary planar structures," J. Opt. Soc. Am. A **15**, 1192–1201 (1998).
24. W. L. Barnes, "Fluorescence near interfaces: The role of photonic mode density," J. Mod. Opt. **45**, 661–699 (1998).
25. J. C. Mertz, "Radiative absorption, fluorescence, and scattering of a classical dipole near a lossless interface: a unified description," J. Opt. Soc. Am. B **17**, 1906–1913 (2000).
26. A. C. Hryciw, Y. C. Jun, and M. L. Brongersma, "Plasmon-enhanced emission from optically-doped MOS light sources," Opt. Express **17**, 185–192 (2009).
27. F. Leblanc, J. Perrin, and J. Schmitt, "Numerical modeling of the optical properties of hydrogenated amorphous-silicon-based *p-i-n* solar cells deposited on rough transparent conducting oxide substrates," J. Appl. Phys. **75**, 1074–1087 (1994).
28. D. Poitras and J. Dobrowolski, "Toward perfect antireflection coatings. 2. Theory," Appl. Opt. **43**, 1286–1295 (2004).
29. M.-L. Kuo, D. J. Poxson, Y. S. Kim, F. W. Mont, L. K. Kim, E. F. Schubert, and S.-Y. Lin, "Realization of a near-perfect antireflection coating for silicon solar energy utilization," Opt. Lett. **33**, 2527–2529 (2008).
30. *ASTM G-173-03* (accessed 30 September 2008). URL `http://rredc.nrel.gov/solar/spectra/am1.5/`.

1. Introduction

While the theoretical limits to the efficiency of single and multijunction solar cells have long been understood [1–3], fabricating cells that approach these limits remains a challenge. Ideally, a single-junction cell absorbs all above-gap photons incident on it and all photogenerated charge carriers are collected, up to the limit imposed by thermodynamics. In practice, harvesting photons in the weakly absorbing spectral range near the band edge requires thick layers, driving up cost, energy of manufacture, and material quality requirements. Surface texturing of thick absorber layers increases the path length of weakly absorbed light inside both indirect and direct gap semiconductors and is routinely employed to enhance absorption in crystalline silicon [4], amorphous silicon [5], and other cells. Much current research, however, focuses on enhancing absorption in thin absorber layers (less than a few micrometers), for which texturing with features larger than the wavelength is not possible.

Thin cells have many potential advantages. Besides requiring less material, thin cells tolerate materials with shorter diffusion lengths, which opens up new classes of materials for thin-film photovoltaics. Furthermore, higher photocarrier concentration in thin absorber layers can potentially boost the open-circuit voltage, thereby increasing efficiency. Stuart and Hall [6–8] demonstrated up to $18\times$ absorption enhancement near $\lambda = 800$ nm in a silicon photodetector caused by a layer of sub-wavelength silver particles spaced from the front surface of the semiconductor by a thin dielectric layer. A similar approach has been used on amorphous silicon [9]

#116570 - $15.00 USD Received 1 Sep 2009; revised 10 Oct 2009; accepted 11 Oct 2009; published 3 Nov 2009

and GaAs [10] absorbers. Recently, Catchpole and coworkers have found similar enhancements in silicon-on-insulator solar cells using the same approach: thin silver films are annealed to produce nanoparticles on the front surface [11, 12]. Above the plasmon resonance, however, these particles exhibit a Fano resonance that serves to reduce absorption in the blue, indicating that the particles would be more beneficial decorating the back surface. [13]

A structured metal layer at the back of the absorber represents another approach to persuading light to propagate parallel to the surface. Using two-dimensional finite-difference-time-domain (FDTD) simulations, Ferry *et al.* have observed absorption enhancement from coupling to waveguide modes caused by sub-wavelength metallic grooves and ridges in thin layers of silicon and GaAs backed with silver [14]. Furthermore, for a range of ridge heights and widths, the scattering pattern of isolated structures is essentially dipolar [15] and the scattering cross section of ridges may be several times their geometric cross section. These results motivate the current study in which we use point dipoles to model ridges or other sub-wavelength objects with high dielectric contrast embedded in the semiconducting absorber layer. We neglect, to a first approximation, their effect on the guided modes of the multilayer structure, which may otherwise include absorbing layers, antireflection layers, in addition to the optically thick metallic substrate layer. The dipoles scatter light into both radiative modes (within the escape cone) and guided modes, including the surface plasmon polariton (SPP) mode localized at the metal/semiconductor interface. Within this simplified semi-analytical model, we seek to understand

- the fraction of power in a guided mode that is absorbed in the semiconductor;
- where the dipoles should be positioned for maximum absorption in the semiconductor; and
- the greatest absorption enhancement possible through this scattering mechanism.

2. Method

Our approach proceeds in four steps. First, we find the fraction of the power in each guided mode of a given multilayer structure that is absorbed in each layer. After all, this method will be useful only if the scattering into guided modes serves to enhance absorption in the semiconductor, not the metallic substrate. Second, for a given position and orientation of an embedded dipole we compute the fraction of light scattered by the dipole that is coupled into both radiating modes and guided modes, taking proper account of the reflections at all the interfaces of the multilayer structure. That is, we neglect any direct coupling between dipoles. Although the plasmon resonance frequency of metal nanoparticles is strongly affected by another metal nanoparticle within a few nanometers, we explore here separations of hundreds of nanometers. At these distances, direct dipole-dipole coupling should be negligible. Third, power scattered into each mode is propagated (incoherently) from the scattering dipole to the nearest neighbor dipole a distance L away, keeping track of the portion absorbed in each layer. This dipole then scatters a portion of the power incident on it, leaving the remainder in the various guided modes. The infinite series of subsequent scattering events in this diffusion process is summed to yield the total absorption in each layer, as well as the portion that escapes into the incident medium, for unit intensity scattered by the first dipole. This approach is surely incorrect at any particular wavelength, for which well-defined phase relationships exist between the various scattered waves. However, for broadband excitation in structures with a variety of separations between dipoles, it should capture the average aggregate behavior. Fourth, we estimate the fraction of light incident on the structure at given polarization and angle that scatters in the first step of the diffusion process, from which it is possible to calculate the total absorption in each layer.

#116570 - $15.00 USD Received 1 Sep 2009; revised 10 Oct 2009; accepted 11 Oct 2009; published 3 Nov 2009

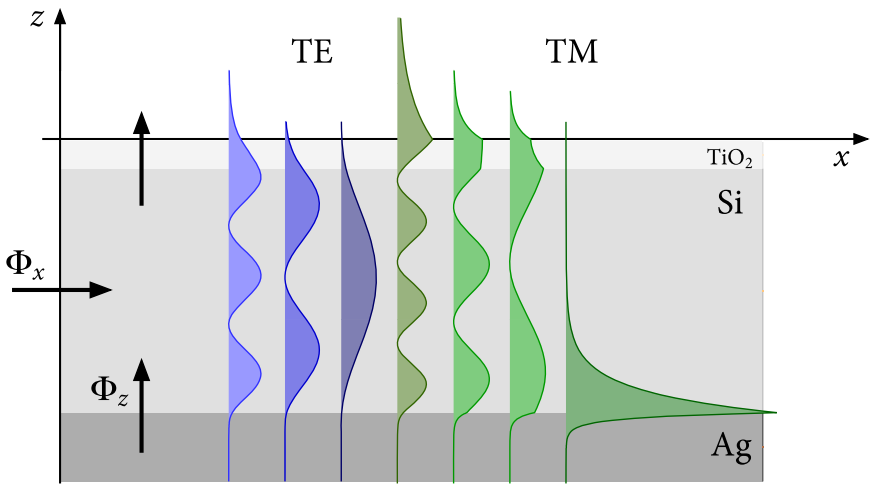

Fig. 1. A multilayer structure with an antireflection-coated silicon absorbing layer on top of an optically thick layer of silver. Absorption in each layer is determined by integrating the power flux through the $x = 0$ plane and through the constant-z interfaces between layers. The illustrated modes have been calculated for a 500-nm Si layer on Ag, with a 56-nm TiO_2 layer on top, at $\lambda = 1100$ nm.

2.1. Absorption in Guided Modes

We assume that the structure may be modeled as having plane, parallel layers of homogeneous and isotropic dielectric properties. That is, we will assume that, for purposes of finding the guided modes of the multilayer structure, we may neglect the ridges or other intrusions that function as dipole scattering sources. We may then solve for the bound modes at a given frequency by requiring the fields to decay exponentially in the incident medium and the substrate.

A monochromatic wave of angular frequency ω inside a homogeneous nonmagnetic medium of (complex) refractive index n satisfies the Helmholtz equation,

$$(\nabla^2 + n^2\tilde{\omega}^2)\mathbf{E}(\mathbf{r},t) = 0 \tag{1}$$

where $\tilde{\omega} = \omega/c$ and c is the speed of light in vacuum. Plane wave solutions to this equation take the form

$$\mathbf{E}(r,t) = \mathbf{E}\exp[i(\mathbf{k}\cdot\mathbf{r} - \omega t)] \tag{2}$$

in which the wave vector $\mathbf{k} \equiv \mathbf{u}\tilde{\omega}$ must satisfy the condition

$$\mathbf{u}\cdot\mathbf{u} = n^2 \tag{3}$$

Boundary conditions at each interface may be satisfied only if u_x is common to all layers, which is Snel's law [16]. In a layer of refractive index n_j, Eq. (3) gives the magnitude of the normal component of the wave vector:

$$u_{z,j} = (n_j^2 - u_x^2)^{1/2} \tag{4}$$

where we take the root having positive imaginary component, and the two linearly independent plane-wave solutions to Eq. (1) are

$$\mathbf{E}_\pm(\mathbf{r},t) = \mathbf{E}_\pm\exp[i\tilde{\omega}(u_x x \pm u_z z) - i\omega t] \tag{5}$$

#116570 - $15.00 USD Received 1 Sep 2009; revised 10 Oct 2009; accepted 11 Oct 2009; published 3 Nov 2009

For real $u_x < 1$, the wave may propagate in the vacuum outside the multilayer; for real $u_x > 1$, or if u_x has an imaginary component, the mode decays exponentially in the vacuum; if the substrate is absorbing, or if $u_x > n_{\text{substrate}}$, then the mode is confined and propagates parallel to the surface. Eigenvalues of u_x are found using the standard transfer matrix formalism [17] to compute the fields in the incident medium corresponding to a purely decaying exponential in the substrate, and requiring the exponentially growing field to vanish.

By momentum conservation, a plane wave incident at any angle from vacuum does not couple to guided modes; however, a scatterer in or near the multilayer can launch a guided wave. We would like to know what fraction of the guided wave's power is absorbed in each layer of the structure. As discussed in the Appendix, this may be computed by integrating the time-averaged Poynting vector over the boundaries of each layer and the plane at $x = 0$. As an example, consider the structure illustrated in Fig. 1, which shows a 500-nm Si layer on an optically thick Ag layer, covered with a 56-nm antireflection layer of TiO_2. The illustrated modes for $\lambda = 1100$ nm are shown with increasing $\mathrm{Re}\, u_x$ from left to right, TE modes on the left and TM modes on the right. For the SPP mode at the far right, the fraction of power absorbed in the silicon layer is 0.35%, with the remainder absorbed in the silver. Thus, 1100-nm light coupled into the SPP mode serves almost exclusively to heat the silver layer.

On the other hand, absorption in Si at this wavelength is quite weak. The fraction of light absorbed in propagating across a 500-nm layer (in the absence of scatterers) is $1 - e^{-\alpha d} \approx \alpha d = 0.052\%$, so that nearly 7 times more energy is absorbed in the silicon layer in the SPP mode than in a single traversal of the layer at normal incidence, provided that the wave does not scatter out of the mode. We call this ratio the absorption enhancement η of the mode. Taking the ratio to the absorption of a single pass at normal incidence facilitates a comparison to the ergodic limit, first computed by Yablonovitch and Cody, to estimate absorption enhancement in thick silicon layers with roughened surfaces [18–20]. The ergodic limit assumes that absorption is very weak ($\alpha d \ll 1$) and that scattering is sufficient to produce an isotropic photon gas inside the semiconducting slab. Because of the large refractive index of the semiconductor, most of the light incident on the front interface from within the slab is totally internally reflected, so that the average ray makes $2n^2$ traversals of the layer. Furthermore, the average traversal has length $2d$. In the weak absorption limit, therefore, absorption is $4n^2\alpha d$, which is enhanced by a factor of $4n^2$ with respect to a single pass through the layer at normal incidence, αd.

Other modes exhibit significantly greater enhancement. From left to right, the transverse-electric modes (TE or *s*-polarized modes with **E** perpendicular to the plane of incidence) have enhancements η of 73, 166, and 542, while the transverse magnetic (TM or *p*) modes have enhancements of 39, 43, and 76. That is, 28.3% of the energy in the fundamental TE mode is absorbed in the silicon layer, despite the very weak absorption coefficient ($n_{\text{Si}} = 3.547 + 9.14 \times 10^{-5} i$). This enhancement arises because the mode energy is concentrated in the silicon layer, not in the silver substrate, and *assumes that the light does not scatter out of the mode*. Since absorption is proportional to $\varepsilon'' |\mathbf{E}|^2$, where ε'' is the imaginary part of the dielectric constant, minimizing the field in the metal minimizes Joule losses.

Figure 2 shows the absorption enhancement η in both TM and TE modes for (bare) silicon layers of various thicknesses and 900 nm $\leq \lambda \leq$ 1100 nm. The enhancement is plotted against the fraction absorbed in the silicon layer. The thickness of the silicon layer is represented by the size of the dot, ranging from 100 to 1000 nm; the wavelength is indicated by the dot's color. The TM modes separate into two regions, SPP modes and "photonic" modes, that show distinctly different dependence on layer thickness. The SPP modes lie below enhancements of about 30 and below a fraction absorbed in the silicon of roughly 6%. Since the SPP mode is localized near the Si/Ag interface, increasing the thickness of the layer has almost no effect on the fraction absorbed in the silicon; it simply reduces the enhancement compared to a single

#116570 - $15.00 USD Received 1 Sep 2009; revised 10 Oct 2009; accepted 11 Oct 2009; published 3 Nov 2009

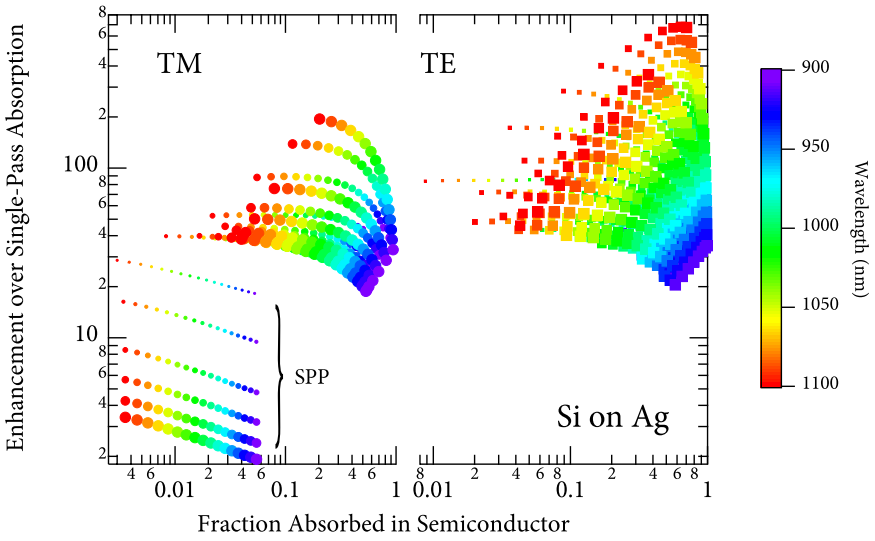

Fig. 2. Absorption enhancement η in a silicon layer on silver compared to a single pass at normal incidence for TM modes (left panel) and TE modes (right panel) as a function of the fraction of energy absorbed in the silicon layer. The marker size shows the thickness of the silicon layer from 100 to 1000 nm and color indicates the wavelength. The SPP mode shows significantly smaller enhancement than other modes, decreasing with increasing layer thickness. For the photonic modes, the absorption enhancement tends to rise with layer thickness. Note that the calculation here assumes that light does not scatter out of the mode.

pass through the layer, since thicker layers absorb more.

By contrast, for the photonic modes, increasing the layer thickness increases both the fraction absorbed in the semiconductor and the absorption enhancement. These modes satisfy $u'_x < n'_{\mathrm{Si}}$, where primes denote the real part; we call them "photonic" due to their resemblance to the modes of dielectric waveguides. The enhancement grows faster than linearly with the layer thickness because the magnitude of the exponentially decaying field in the metal decreases as the semiconductor thickness increases. At wavelengths near 1 μm, the fraction absorbed within the semiconductor exceeds 20%. TE modes exhibit even greater enhancements, as shown in the right panel of Fig. 2. For layers of roughly 1-μm thickness, the enhancement in the most favorable fundamental TE mode exceeds 600. This is more than 12 times better than the ergodic limit, although the ergodic limit includes scattering out of guided modes, of course. As in the ergodic case, large values of η arise from very long propagation distances in the silicon layer. As an example, the fundamental TE mode at $\lambda = 1100$ nm for a 1-μm Si layer on Ag has $u_x = 3.509 + 1.31 \times 10^{-4} i$, from which we deduce a decay length of $\ell = \lambda/4\pi u''_x = 670$ μm.

2.2. Dipole Scattering

To model scattering into the various guided modes of multilayer structures, we consider a point dipole embedded in a non-absorbing dielectric layer of the structure (including the incident medium or substrate, if desired). We use a method devised originally by Sipe [21], to investigate modifications to emission from atoms or molecules near a metallic plane. The method expands the dipole field in plane waves and assumes a local dielectric response in the metal, which is satisfied for dipoles at least 10 nm from the metal [22], and has been applied in various forms to a variety of radiation problems [11,23–26]. If we may neglect nonradiative loss in the dipole,

#116570 - $15.00 USD Received 1 Sep 2009; revised 10 Oct 2009; accepted 11 Oct 2009; published 3 Nov 2009

and call the decay rate of the dipole in an infinite slab of the dielectric γ_{free}, then the normalized decay rate of the dipole is [26]

$$\hat{\gamma} = \frac{\gamma}{\gamma_{\text{free}}} = \int_0^\infty \frac{1}{\mathscr{P}_{\text{free}}} \frac{d\mathscr{P}}{du_x}\, du_x \tag{6}$$

where the normalized decay rate density is given by

$$\frac{1}{\mathscr{P}_{\text{free}}} \frac{d\mathscr{P}}{du_x} = \frac{3}{2n^3} \text{Re}\left\{ \frac{u_x}{u_z} \left[u_x^2 \tilde{r}_\perp^p \cos^2\theta_d + \frac{\sin^2\theta_d}{2} \left(n^2 \tilde{r}_\parallel^s + u_z^2 \tilde{r}_\parallel^p \right) \right] \right\} \tag{7}$$

$$\tilde{r}_\perp^p = \frac{\left[1 + r_-^p \exp(2ik_z d_-)\right]\left[1 + r_+^p \exp(2ik_z d_+)\right]}{1 - r_-^p r_+^p \exp(2ik_z d)} \tag{8}$$

$$\tilde{r}_\parallel^s = \frac{\left[1 + r_-^s \exp(2ik_z d_-)\right]\left[1 + r_+^s \exp(2ik_z d_+)\right]}{1 - r_-^s r_+^s \exp(2ik_z d)} \tag{9}$$

$$\tilde{r}_\parallel^p = \frac{\left[1 - r_-^p \exp(2ik_z d_-)\right]\left[1 - r_+^p \exp(2ik_z d_+)\right]}{1 - r_-^p r_+^p \exp(2ik_z d)} \tag{10}$$

The dipole's axis makes angle θ_d with respect to the normal and is located in a layer of refractive index n at d_- (d_+) from the adjacent layer at smaller (greater) z, $d = d_- + d_+$ is the layer thickness, and $k_z = u_z \widetilde{\omega}$ is the normal component of the wave vector in the dipole layer. See the inset in Fig. 3. The p-polarized amplitude reflection coefficient for all the layers at $z \geq d$ is denoted r_+^p, and similarly for the other reflection coefficients. For the weakly absorbing region, we use a purely real index for the semiconductor for purposes of computing $\hat{\gamma}$. When the semiconductor absorption is too large to ignore, we surround the dipole with lossless "sliver" layers 10-nm thick having the same value of n' as the semiconductor.

As illustrated in the top panel of Fig. 3, the normalized decay rate density at $\lambda = 1100$ nm of a 1-μm Si layer on Ag exhibits six sharp peaks, corresponding to photonic modes, and one broad peak near $u_x = 4$, corresponding to the SPP mode. This panel shows coupling for a dipole oriented perpendicularly to the plane of the layers (i.e., for which $\theta_d = 0$), embedded in the silicon layer at 50 nm (200 nm) from the Ag substrate in the solid (dotted) trace. The area under the SPP peak for $d_- = 50$ nm is 2.2, meaning that the rate at which this dipole radiates into the SPP mode is 2.2 times its rate of emission into 4π steradians in an infinite block of silicon. For $d < 100$ nm, the SPP mode dominates emission into TM modes for both perpendicular and parallel dipoles. Hence, the field is concentrated in the metal substrate, leading to poor absorption enhancement in the semiconductor. We are not so much interested in the rate as in the fraction of power that goes into each of the modes, including radiative modes, for which $u_x < 1$. By computing the area under each peak, we find that the fraction of power radiated out of the multilayer for this dipole is 0.04%, while that going into the SPP mode is 95.7%. When the dipole is moved to $d_- = 200$ nm, these fractions change to 0.03% and 8.3%. In this position, therefore, the great majority of the power goes into photonic modes that exhibit large absorption enhancements.

A dipole oriented parallel to the layers ($\theta_d = \pi/2$) couples to both p- and s-polarized modes, as illustrated in the lower two panels of Fig. 3. To determine the fraction ρ_j of emission into mode j, we consider both $p_\parallel$ and $s_\parallel$ together, normalizing against the combined area under both curves. We can now calculate how the scattered light couples to each mode (ρ_j) and the fraction of power in mode j that is absorbed in each layer. Note that ρ_0 represents the fraction of power that couples to radiating modes.

#116570 - $15.00 USD Received 1 Sep 2009; revised 10 Oct 2009; accepted 11 Oct 2009; published 3 Nov 2009

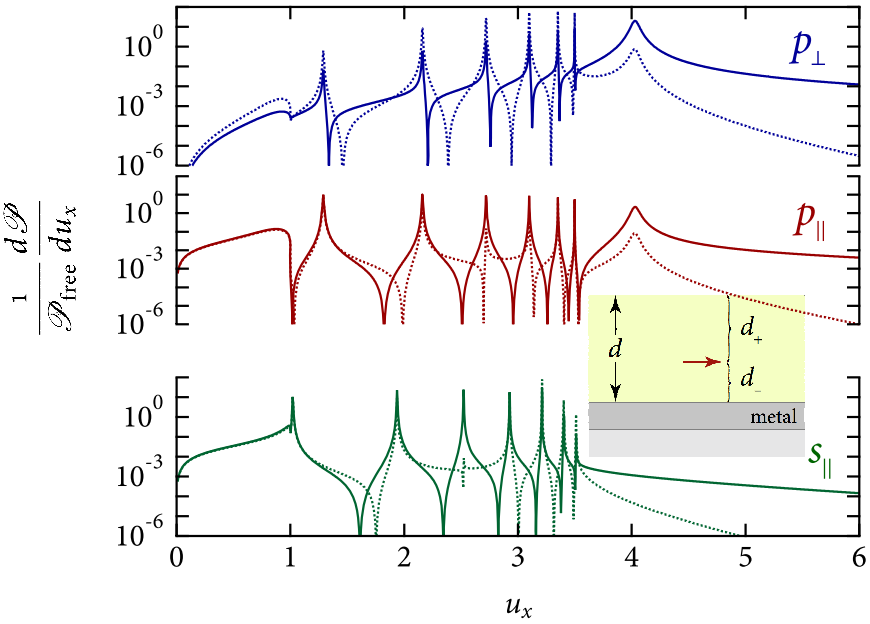

Fig. 3. Normalized decay rate at $\lambda = 1100$ nm for a dipole in a $d = 1$-μm silicon layer a distance $d_- = 50$ nm from a silver substrate (solid traces) and 200 nm from the silver layer (dotted traces) as a function of the normalized wave vector component parallel to the surface. The inset illustrates the structure.

2.3. Multiple Scattering

We now consider the extent to which scattering *out* of guided modes compromises the very large absorption enhancements of guided modes. Light that scatters from a dipole at distance d_- from the metal/semiconductor interface into a given guided mode will also efficiently scatter out of that mode on encountering a second dipole that is also at d_-. We assume that the phase of the light is effectively scrambled on scattering, so that we may treat the propagation in each mode—and the scattering at the next dipole—incoherently. This approach was originally developed by Leblanc *et al.* [27] to describe the propagation of light in multilayer amorphous silicon structures with rough interfaces, and has been used recently by Catchpole and coworkers to model absorption enhancement from metal nanoparticles on the surface of a multilayer structure [12]. As in the latter work, we take proper account of the discrete modes of multilayer structures, but consider in this work the application of the theory to dipole scattering centers embedded within an absorbing layer of the structure.

The approach is illustrated in Fig. 4. Let $\Lambda(\lambda)$ represent the fraction of light of wavelength λ that is scattered by a given dipole, and L be the typical distance between the dipoles. We consider unit intensity that leaves the dipole, which divides into a fraction ρ_0 in the escape cone, and ρ_j in guided mode j. If $f_{\beta j}$ is the fraction of power in mode j that is absorbed in layer β, and $\alpha_j = 2u_x''\widetilde{\omega}$ is the decay constant of mode j, then the power from mode j absorbed in layer β between dipoles is

$$A_{\beta j}^{(0)} = f_{\beta j}\left(1 - e^{-\alpha_j L}\right)\Sigma_j^{(0)} = f_{\beta j} l_j \Sigma_j^{(0)} \tag{11}$$

where $\Sigma_j^{(0)} = \rho_j \Sigma^{(0)}$ is the fraction of the initially scattered flux $\Sigma^{(0)}$ that couples into mode j and l_j is the fraction of light in mode j that is absorbed on propagating a distance L. The total

#116570 - $15.00 USD Received 1 Sep 2009; revised 10 Oct 2009; accepted 11 Oct 2009; published 3 Nov 2009

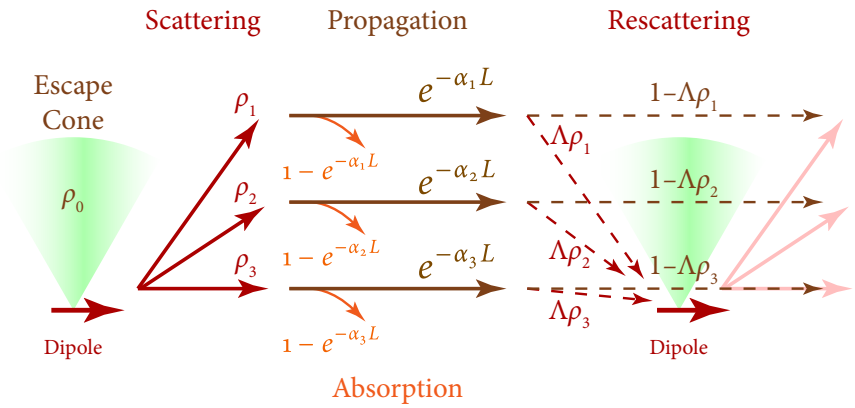

Fig. 4. Diffusion model of light propagation inside the multilayer structure. Light is scattered by the dipole on the left into the escape cone, with fraction ρ_0, and into guided modes with fractions ρ_j. Each guided mode propagates a distance L to the next dipole, with loss in each absorbing layer dependent on the mode. At the next dipole, a fraction $\Lambda\rho_j$ of the remaining light scatters. Its power is added to the unscattered light in each mode.

power absorbed in layer β from all guided modes propagating over the distance L is

$$A_\beta^{(0)} = \sum_{j=1}^{N} A_{\beta j}^{(0)} \tag{12}$$

where the sum is over the N guided modes.

The scattered power in mode j now arrives at the next dipole, where it has probability $\Lambda\rho_j$ of scattering. The remaining power, $(1-\Lambda)\rho_j$, continues to propagate in mode j past this dipole, a portion being absorbed in each layer until it encounters the next dipole in the next step of the energy diffusion process. Thus, we take the scattering matrix to be

$$\mu_{ij} = \Lambda\rho_i\rho_j + \delta_{ij}(1-\Lambda)\rho_j \tag{13}$$

with δ_{ij} being the Kronecker delta. This expression for the $(N+1)\times(N+1)$ matrix μ_{ij} is constructed to conserve power and to ignore interference between fields arriving at the dipole from different modes (and the incident wave). If the dipoles are not ideal, but convert a fraction $\hat{g}$ of the scattered power into heat, then μ_{ij} becomes

$$\mu_{ij} = \Lambda\rho_i\rho_j(1-\hat{g}) + \delta_{ij}(1-\Lambda)\rho_j \tag{14}$$

The flux that scatters into mode i at the second scattering event is thus

$$\Sigma_i^{(1)} = \sum_{j=1}^{N} (1-l_j)\mu_{ij}\Sigma_j^{(0)} \tag{15}$$

from which we may compute absorptions $A_{\beta j}^{(1)} = f_{\beta j} l_j \Sigma_j^{(1)}$, etc.

The infinite series of scattering events may be conveniently summed [27], yielding the total absorption in each layer. Passing to matrix notation, we may express the flux leaving the nth dipole as

$$\{\Sigma^{(n)}\} = [F]\{\Sigma^{(n-1)}\} = [F]^n\{\Sigma^{(0)}\} \tag{16}$$

#116570 - $15.00 USD Received 1 Sep 2009; revised 10 Oct 2009; accepted 11 Oct 2009; published 3 Nov 2009

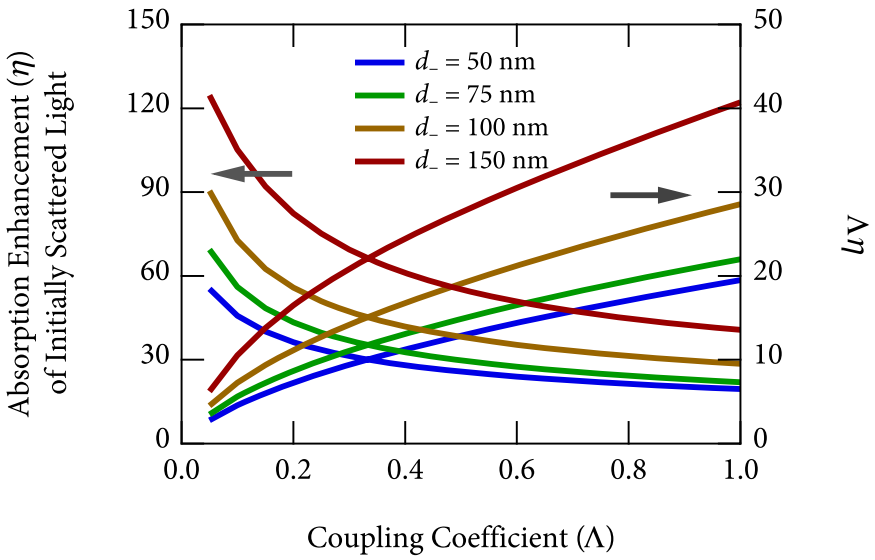

Fig. 5. Band-edge absorption enhancement (η, left axis) of light leaving a dipole a distance d_- from the Ag/Si interface, compared to single-pass absorption for a 200-nm Si layer on Ag, as a function of coupling coefficient Λ ($L = 1$ μm, $\lambda = 1100$ nm). The product $\Lambda\eta$ (right axis) scales the curves assuming that the initial scattering is also Λ.

where $F_{ij} = \mu_{ij}(1 - l_j)$. Then the total absorption in each layer is given by

$$\{A\} = \sum_{n=0}^{\infty} \{A^{(n)}\} = \sum_{n=0}^{\infty} [f][l][F]^n \{\Sigma^{(0)}\} = [f][l](\quad - [F])^{-1} \{\Sigma^{(0)}\} \tag{17}$$

where $[l]$ has elements $l_{ij} = l_j \delta_{ij}$. Note that $[f]$ is an $M \times (N+1)$ matrix, where M is the number of layers, including both the incident medium and the substrate. Thus, for unit flux leaving the dipole, A_β is the fraction that is absorbed in layer β.

3. Results

Figure 5 illustrates how the coupling coefficient Λ of the dipoles affects absorption enhancement for a 200-nm Si layer on Ag. The dipoles are assumed to be lossless ($\hat{g} = 0$) and spaced $L = 1$ μm apart. Plotted against the left axis for four different positions of the parallel dipoles with respect to the Si/Ag interface is the absorption enhancement η *of the light that initially scatters* as a function of Λ. In all cases the enhancement decreases monotonically with Λ, because with increasing Λ the probability of scattering out of a guided mode and into the escape cone increases. Since we consider only the light that has already been scattered into guided modes by the first dipole, scattering reduces the net absorption. Of course, without an initial scattering event, none of the light would enter guided modes in the first place. As a crude in-coupling approximation, if we assume that scattering of the incident wave into guided modes is described by the same coupling coefficient Λ, then $\Lambda\eta$ gives a more realistic estimate of the absorption enhancement. This is plotted for the same four dipole positions against the right axis, and is a monotonically *increasing* function of Λ. As is physically reasonable, regardless of dipole position the greatest enhancement occurs for dipoles that scatter all light incident on them.

Estimating more accurately the fraction of normally incident light that scatters on first encountering the dipoles is quite complicated. In the limit of small Λ, we may treat the dipole

#116570 - $15.00 USD Received 1 Sep 2009; revised 10 Oct 2009; accepted 11 Oct 2009; published 3 Nov 2009

scattering as a weak perturbation and use the fields in the absence of the dipoles to estimate the scattering. In this limit, the reflectivity of the structure is approximately unaffected by the dipoles and can be used to estimate the power participating in the diffusion. The field at the dipole consists in the superposition of the forward- and backward-propagating waves, as may be computed with the transfer matrix method ([17], § 1.6). The strong-coupling limit is more interesting, however. With increasing scattering, the fields inside the multilayer will be perturbed in a complicated way away from their values in the absence of scattering.

In the limit of perfect scattering, the forward-going wave is completely eliminated and the situation becomes simple once again. In this case the reflectivity of a thin slab of lossy dielectric becomes that of an infinitely thick slab, $R_\infty = \left|\frac{n-1}{n+1}\right|^2$, and the field at the dipole located d_+ below the front interface is

$$E(d_+) = E_0 t e^{i\tilde{\omega} n d_+} \tag{18}$$

where n is the complex index of refraction of the dielectric and $t = \frac{2}{n+1}$ is the transmission coefficient of the air/dielectric interface. For a bare 200-nm slab of Si on Ag, this lowers the normal reflectivity at the band edge from 89% to 31%. An effective antireflection coating on the front surface increases this difference.

A 200-nm thick silicon layer has only one TM photonic mode and one TE mode; greater enhancements than shown in Fig. 5 are possible for thicker layers, which can reduce the relative importance of the comparatively lossy SPP mode. Figure 6 shows the absorption enhancement with respect to a single pass at normal incidence of an 800-nm-thick silicon layer on silver as a function of dipole position for wavelengths near the absorption edge at $\lambda \approx 1100$ nm. In this case, the silicon layer is assumed to be covered with a perfect broadband antireflection coating, which eliminates all reflections at the front surface of the silicon (until the angle of incidence for light incident from within the silicon exceeds the critical angle). Recent coating layers of gradually varying index approach this idealized condition [28, 29], which we therefore take as a realistic limit. Furthermore, to explore the limiting enhancement possible with ideal dipoles, we assume $\Lambda = 1$, independent of wavelength.

At any given wavelength, the absorption enhancement oscillates with dipole position, reflecting the changes in mode coupling that depend on the dipole position and orientation (which here is assumed parallel to the interfaces). We might expect that enhancement would be greatest for dipole positions that couple most strongly to the TE modes that minimize the absorption in the metal. To investigate, we evaluate the coupling fractions into the various modes for dipoles at 200 nm from the Ag, where enhancement at 1100 nm is minimum, and at 300 nm from the Ag interface, near the global maximum. The modes of this structure at $\lambda = 1100$ nm, for which the fraction of power absorbed in a single pass at normal incidence is $\alpha d = 8.4 \times 10^{-4}$, are shown in Fig. 7, along with the fraction absorbed in the silver and the silicon for each mode. The silicon fraction ranges from 0.35% for the SPP mode, to 56.1% for the fundamental TE mode. In addition, the coupling fractions to each mode are shown at the right of each figure for two positions of the dipoles, $d_- = 200$ nm (red), corresponding to an approximate minimum in enhancement, as seen in Fig. 6, and $d_- = 300$ nm (green), corresponding to a maximum.

Several remarks are in order. First, the coupling fractions confirm an intuitive interpretation of mode coupling: it scales with the magnitude squared of the field component parallel to the dipole, at the position of the dipole. Second, parallel dipoles this far from the metal interface couple much more strongly to TE modes than to TM modes, and coupling to the SPP mode is negligible. Third, *the most significant coupling difference between these two positions is the fraction coupled to the escape cone at each scattering event*. At the enhancement minimum, 11.2% of the scattered light couples to the escape cone, whereas at $d_- = 300$ nm only 0.4% escapes. We note again that this behavior describes dipoles oriented parallel to the layers; perpendicular dipoles might show less modulation. Successive peaks in the enhancement at 1100

#116570 - $15.00 USD Received 1 Sep 2009; revised 10 Oct 2009; accepted 11 Oct 2009; published 3 Nov 2009

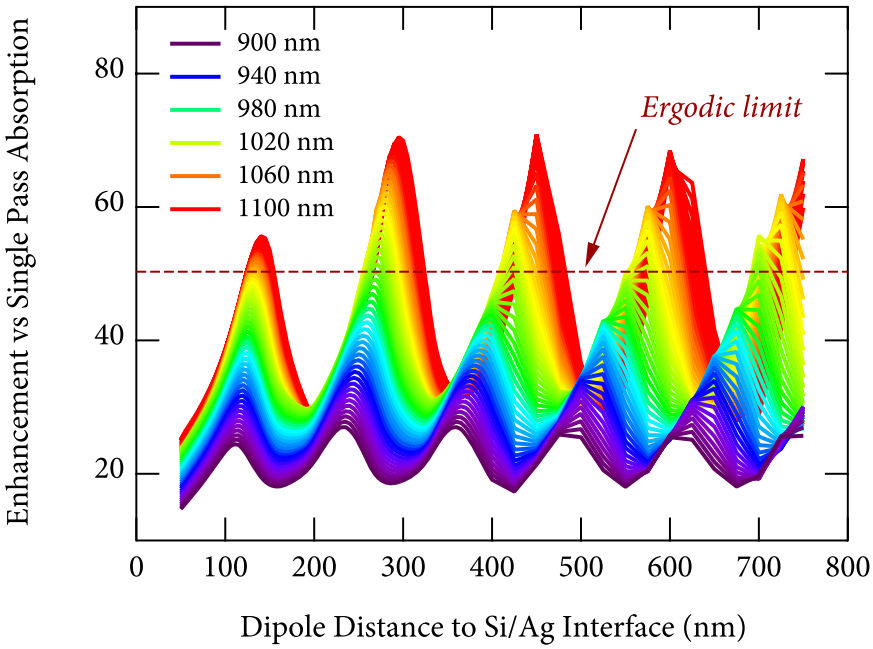

Fig. 6. Absorption enhancement of light near the band edge caused by dipoles parallel to the surface of an 800-nm Si layer on Ag. The silicon is covered with a perfect antireflection coating, $\Lambda = 1$, and $L = 1\ \mu$m. The dashed line shows the ergodic limit for $\lambda = 1100$ nm in a thick silicon layer. Note that a higher density of points has been computed for $d_- < 400$ nm.

nm are separated by about 150 nm, which is half the wavelength in the silicon, $\lambda/n' = 310$ nm. At positions where emission from the dipole towards the silver reflects and returns to the dipole out of phase with the forward emission, near perfect destructive interference produces a minimum in emission, thanks to the high reflectivity of the Si/Ag interface. [Note that with the perfect antireflection coating, there is no reflection at the upper silicon surface.] Fourth, dispersion shifts the position of the maxima increasingly with d_-, so smaller values of d_- lead to large enhancements over a broader range of wavelengths. However, coupling to the SPP mode leads to smaller enhancement at $d_- = 135$ nm than at $d_- = 290$ nm so that the greatest integrated enhancement in this structure requires $d_- \approx 260$ nm.

The greatest enhancement at the band edge for this structure is about 70 (Fig. 6). This is considerably greater than the $4n^2 = 50.3$ enhancement of the ergodic limit, which assumes that absorption is negligible. Actually, $4n^2$ is the limit for bulk layers; as Stuart and Hall have shown, it is somewhat reduced in thin layers [6]. Over a range of wavelengths near the band edge, ideal dipole scattering with properly positioned strong scatterers exceeds the ergodic limit by a wide margin.

While large absorption enhancements near the band edge help improve a cell's efficiency, of greater significance is the total absorption integrated from the band edge to the UV limit of the solar spectrum, which we take to be $\lambda_{UV} = 340$ nm (3.65 eV). The spectrally integrated absorption efficiency (IAE) for a given spectral range is then the ratio of the number of photons absorbed in the semiconductor to the total number incident, per unit area.

For short wavelengths, absorption is strong enough to make enhancement mechanisms (texturing or dipole scattering) unnecessary, since most photons are absorbed before arriving at the metal interface. It is illustrative, therefore, to show the limiting IAE for the spectral regions both

#116570 - $15.00 USD Received 1 Sep 2009; revised 10 Oct 2009; accepted 11 Oct 2009; published 3 Nov 2009

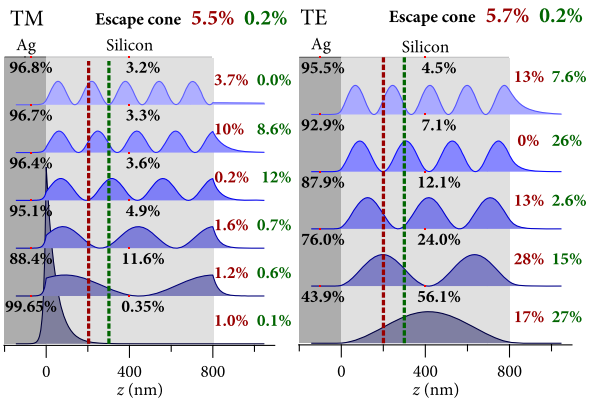

Fig. 7. TM (left) and TE (right) modes of an 800-nm Si layer on Ag at $\lambda = 1100$ nm. The shaded curves show the magnitude squared of the parallel component of electric field, and have equal area. The black numbers in each layer show for each guided mode the fraction absorbed in the layer (e.g., for the SPP mode at the lower left, 0.35% is absorbed in the silicon and 99.65% is absorbed in the silver). The fraction of light coupled into each mode for a parallel dipole positions 200 nm (300 nm) from the Ag layer is shown in red (green) at the right of each figure; the fraction coupled into the escape cone is shown at the top.

near the band edge and up to λ_{UV}. Figure 8 shows these efficiencies for several semiconductor layer thicknesses in two weakly absorbing (Si and Ge) and two strongly absorbing (a-Si:H and GaAs) semiconductors. In all cases the upper surface is perfectly antireflection coated and the metallic substrate layer is silver. For Si and Ge, the dipole is at $d_{-} = 200$ nm from the metal interface. For the thinner layers of a-Si:H and GaAs, d_{-} is the smaller of $d/2$ and 100 nm, where d is the semiconductor layer thickness, to keep the dipoles from approaching the front surface.

Dipole scattering significantly enhances absorption in both weak and strong absorbers. Although the proportional increase in integrated IAE is greater for the weak absorbers (13.9 for Si and 6.8 for Ge versus 4.4 for a-Si:H and 5.0 for GaAs at the smallest thickness considered for each material), the absolute increase is greater for the strong absorbers. A 100-nm a-Si:H layer with ideal scatterers spaced 500-nm apart absorbs 87% of the incident photons in the range 340 nm $\leq \lambda \leq$ 840 nm. Without the scatterers (*i.e.*, in a structure with plane parallel interfaces), it would take a layer 7 times thicker to achieve the same absorption.

4. Discussion

We aim here to understand the theoretical limit to absorption enhancement in a thin metal-backed layer caused by dipole scatterers embedded in the absorbing layer. Accordingly, we have made a number of idealizations, some of which may be difficult to achieve experimentally. Specifically, we have assumed that:

1. the dipoles are strong enough and spaced closely enough such that they scatter all incident light ($\Lambda(\lambda) = 1$);
2. the dipoles do not significantly perturb the guided modes of the multilayer structure;
3. the multiple scattering at a given wavelength may be treated incoherently;
4. the dipoles are lossless scatterers ($\hat{g} = 0$);

#116570 - $15.00 USD Received 1 Sep 2009; revised 10 Oct 2009; accepted 11 Oct 2009; published 3 Nov 2009

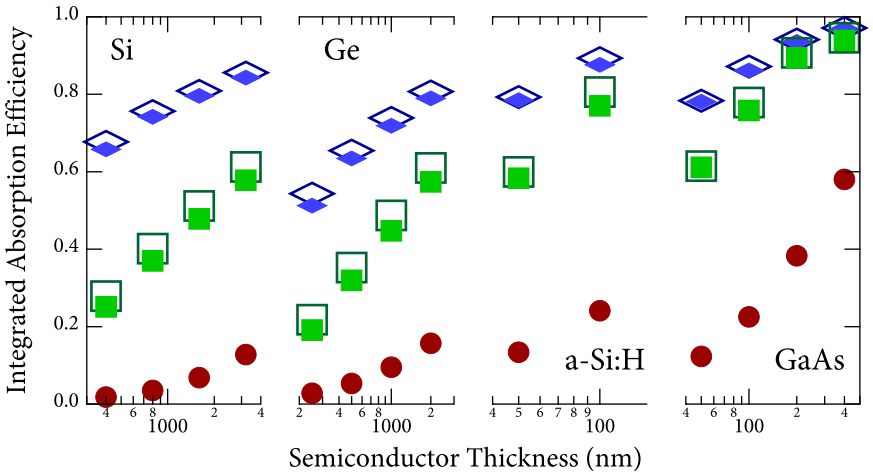

Fig. 8. Limiting integrated absorption efficiency (IAE) for thin layers of silicon, germanium, amorphous silicon, and gallium arsenide on optically thick Ag layers illuminated with the AM1.5G spectrum [30]. The squares show the IAE for the spectral range near the band edge ($\frac{3}{4}\lambda_g \leq \lambda \leq \lambda_g$), whereas the circles show the IAE for the same spectral range in the absence of dipole scatterers. The diamonds show IAE for the full spectrum ($\lambda_{UV} \leq \lambda \leq \lambda_g$). The semiconductor layers are covered with a perfect antireflection coating. The dipoles are separated by 500 nm for the filled symbols and by 1000 nm for the open symbols.

5. losses in the optically thick metal layer on the substrate are described by the (bulk, local) complex dielectric function; and

6. the upper surface of the absorber is covered by a perfect antireflection coating.

Given these assumptions, we find that for both indirect-gap materials, such as silicon and germanium, and direct or quasi-direct-gap materials, such as gallium arsenide and amorphous silicon, lossless dipole scatterers that interact strongly with above-gap radiation can very significantly enhance absorption in the semiconductor, even when Joule losses in the metal substrate layer are accounted for. But, are the assumptions reasonable?

Approaching the strongly coupled limit ($\Lambda = 1$) may be possible, at least at selected wavelengths. Using Mie theory [15], we find that silver spheres with 50-nm radius embedded in silicon have a scattering cross section $Q_{sca} = 6.6$ times their geometric cross section at $\lambda = 880$ nm, and an average Q_{sca} greater than 5 over the range 800–1100 nm. Silver ridges 100-nm wide and spaced about 500 nm apart may scatter a fraction approaching unity of incident plane waves, at least for wavelengths in the infrared. As shown in Fig. 8, while scatterers spaced 1 μm apart are more efficient, the difference compared to 500-nm spacing is modest. It may be difficult to realize appropriately spaced embedded scatterers without introducing excessive surface recombination, and without strongly perturbing the multilayer modes we have assumed. Metallic ridges 50-nm tall in a layer 100-nm thick will produce significant Fabry-Pérot resonances that alter the radiative density of states. However, this effect would be sharply reduced for thicker absorbing layers, such as the 800-nm layers of Fig. 7. Thin metallic islands on dielectric pedestals penetrating into the semiconductor might alter the pure multilayer modes less than ridges, yet maintain their large scattering efficiency.

Our treatment of the dipoles as independent scatterers is supported by absorption enhancement caused by silver islands on thin silicon layers [11]. As regards the fourth assumption,

#116570 - $15.00 USD Received 1 Sep 2009; revised 10 Oct 2009; accepted 11 Oct 2009; published 3 Nov 2009

we have focused on metallic scatterers because strong plasmon resonances enable these structures to have very large scattering cross sections, as indicated above. Furthermore, scattering dominates absorption at these sizes. For the same 800–1100 nm range that has $\overline{Q}_{\text{sca}} = 5.1$, the dimensionless total extinction cross section is $Q_{\text{ext}} = 5.76$, indicating that 8 times more power is scattered than absorbed in the metal. We have calculated principally for silver, which has the least loss of any metal across the relevant spectral range. Less expensive and more abundant metals, such as copper, may be worth exploring, particularly for infrared application where losses are quite similar to silver. Furthermore, we have assumed a single value for the coupling coefficient Λ in producing Fig. 8, although scattering efficiency is apt to decrease with wavelength into the visible. We have also taken Λ independent of the position of the dipoles with respect to the metal/absorber interface. This assumption is bolstered by looking at the integrated decay rate, $\hat{\gamma}$, for perpendicular and parallel dipoles as a function of d_{-}. For d_{-} greater than about 80 nm, $\hat{\gamma}$ is within $\approx$25% of unity, independent of the dipole position. So, while the fraction coupling to each mode changes with d_{-}, the total coupling is fairly constant. Furthermore, variations in $\hat{\gamma}$ are significant only in comparison to alternative energy pathways, which we take as negligible. We will explore the influence of absorption in the dipoles ($\hat{g} > 0$) and declining scattering with wavelength in a subsequent publication.

The fifth assumption is entirely reasonable, as we find that the scatterers should be placed much more than 10 nm from the metal plane, far enough that surface effects are entirely negligible. Finally, efficient absorption in any geometry requires minimizing reflection losses, and achieving optimal efficiency demands an ideal antireflection coating. Whether broadband AR coatings will be economically feasible is an interesting but separate question. Regardless, the dipole-scattering mechanism enhances absorption whether front-surface reflections are suppressed or not.

5. Conclusion

We have elaborated a quasi-analytic theory of absorption in multilayer structures with independent embedded dipole scatterers. Unlike full-field simulations using FDTD, the method uses experimental dielectric functions and runs quite quickly, allowing us to explore parameter space more efficiently. In this paper, we have focused on structures with optically thick metal back planes, which support both plasmonic and photonic guided modes. We find that while absorption losses at optical frequencies are greatest in SPP modes, they do not spoil the very significant absorption enhancement in a broad variety of structures. When these ideal dipole scatterers couple strongly enough to scatter essentially all incident light, yet are spaced roughly 500-nm part, they enable absorption of greater than 85% of above-gap solar radiation in AR-coated thin absorber layers.

6. Appendix

The fraction of the power in a guided mode that is absorbed in each lossy layer may be computed by considering the power flux into each layer through the plane at $x = 0$ and between layers through the interfaces that separate them, as illustrated in Fig. 1. The average power per unit area carried by the monochromatic electromagnetic field is given by the average Poynting vector, $\mathbf{S} = \frac{c}{8\pi} \text{Re}\,(\mathbf{E} \times \mathbf{H}^*)$.

Consider a layer bounded below at $z = 0$ and above by $z = d$. A TM-polarized mode has the

#116570 - $15.00 USD Received 1 Sep 2009; revised 10 Oct 2009; accepted 11 Oct 2009; published 3 Nov 2009

form

$$\mathbf{E}(\mathbf{r},t) = \left[E_+\left(\frac{-u_z\hat{\mathbf{x}}+u_x\hat{\mathbf{z}}}{n}\right)e^{ik_z z} + E_-\left(\frac{u_z\hat{\mathbf{x}}+u_x\hat{\mathbf{z}}}{n}\right)e^{-ik_z z}\right]e^{i(k_x x-\omega t)} \tag{19}$$

$$\mathbf{H}(\mathbf{r},t) = -\left(E_+e^{ik_z z}+E_-e^{-ik_z z}\right)ne^{i(k_x x-\omega t)}\,\hat{\mathbf{y}} \tag{20}$$

where the amplitudes $E_\pm$ are those at the back of the layer at $z=0$, and I have taken $\mu=1$. The power flux into the layer along the $x=0$ plane, per unit length in the y direction, is then

$$\Phi_x^{\mathrm{TM}} = \int_0^d S_x\,dz = \frac{c}{16\pi}u_x''\,\mathrm{Re}\left[\frac{n^*u_x}{n}\left\{\frac{|E_+|^2(1-e^{-2u_z''\phi})}{u_z''}+\frac{|E_-|^2(e^{2u_z''\phi}-1)}{u_z''}\right.\right.$$
$$\left.\left.+\frac{2\,\mathrm{Im}(E_+E_-^*)\sin(2u_z'\phi)}{u_z'}+\frac{2\,\mathrm{Re}(E_+E_-^*)[\cos(2u_z'\phi)-1]}{u_z'}\right\}\right] \tag{21}$$

where $\phi=\widetilde{\omega}d=2\pi d/\lambda$, λ is the vacuum wavelength, the field amplitudes $E_\pm$ are those at $z=0$, and the real and imaginary parts of a complex number ζ are represented by ζ' and ζ'', respectively. Similarly, the flux per unit length in the y direction through a plane perpendicular to the z axis for $x\geq 0$ are

$$\Phi_z^{\mathrm{TM}}(z) = \int_0^\infty S_z(z)\,dx = \mathrm{Re}\left\{\frac{cn^*u_z}{16\pi n}\left[|E_+|^2e^{-2k_z''z}-|E_-|^2e^{2k_z''z}+2i\,\mathrm{Im}(E_+E_-^*e^{-2ik_z'z})\right]\right\} \tag{22}$$

We note that in the case of the incident medium (for which $d\to\infty$), the terms involving E_- vanish in a bound mode; in the substrate $E_+=0$.

For a TE mode, the analogous expressions are

$$\mathbf{E}(\mathbf{r},t) = \left(E_+e^{ik_z z}+E_-e^{-ik_z z}\right)e^{i(k_x x-\omega t)}\,\hat{\mathbf{y}} \tag{23}$$

$$\mathbf{H}(\mathbf{r},t) = \left[E_+\left(-u_z\hat{\mathbf{x}}+u_x\hat{\mathbf{z}}\right)e^{ik_z z}+E_-\left(u_z\hat{\mathbf{x}}+u_x\hat{\mathbf{z}}\right)e^{-ik_z z}\right]e^{i(k_x x-\omega t)} \tag{24}$$

$$\Phi_x^{\mathrm{TE}} = \frac{cu_x'u_x''}{16\pi}\left[\frac{|E_+|^2(1-e^{-2u_z''\phi})+|E_-|^2(e^{2u_z''\phi}-1)}{u_z''}\right.$$
$$\left.+\frac{2}{u_z'}\left(\mathrm{Re}[E_+E_-^*]\sin(2u_z'\phi)-\mathrm{Im}[E_+E_-^*][1-\cos(2u_z'\phi)]\right)\right] \tag{25}$$

$$\Phi_z^{\mathrm{TE}}(z) = \frac{c}{16\pi}\left[u_z'\left(|E_+|^2e^{-2k_z''z}-|E_-|^2e^{2k_z''z}\right)+2u_z''\,\mathrm{Im}\left(E_+^*E_-e^{-2ik_z'z}\right)\right] \tag{26}$$

Acknowledgments

This work was supported by Harvey Mudd College and the Department of Energy, under contract DE-FG02-07ER46405. We gratefully acknowledge useful discussions with L. A. Sweatlock.

#116570 - $15.00 USD Received 1 Sep 2009; revised 10 Oct 2009; accepted 11 Oct 2009; published 3 Nov 2009